Long-range plasmonic waveguides with hyperbolic cladding

Viktoriia E. Babicheva,[1,2] Mikhail Y. Shalaginov,[3] Satoshi Ishii,[4] Alexandra Boltasseva,[3,5] and Alexander V. Kildishev[3,*]

[1]*Center for Nano-Optics, Georgia State University, P.O. Box 3965, Atlanta, 30302 GA, USA*
[2]*ITMO University, Kronverkskiy prospekt, 49, St. Petersburg 197101, Russia*
[3]*School of Electrical and Computer Engineering and Birck Nanotechnology Center, Purdue University, 1205 West State Street, West Lafayette, IN 47907-2057, USA*
[4]*International Center for Materials Nanoarchitectonics (MANA), National Institute for Materials Science (NIMS), Tsukuba, Ibaraki 305-0044, Japan*
[5]*DTU Fotonik – Department of Photonics Engineering, Technical University of Denmark, Oersteds Plads 343, Kgs. Lyngby 2800, Denmark*
[*]*kildishev@purdue.edu*

Abstract: We study plasmonic waveguides with dielectric cores and hyperbolic multilayer claddings. The proposed design provides better performance in terms of propagation length and mode confinement in comparison to conventional designs, such as metal-insulator-metal and insulator-metal-insulator plasmonic waveguides. We show that the proposed structures support long-range surface plasmon modes, which exist when the permittivity of the core matches the transverse effective permittivity component of the metamaterial cladding. In this regime, the surface plasmon polaritons of each cladding layer are strongly coupled, and the propagation length can be on the order of a millimeter.

References and links

1. G. T. Reed, G. Mashanovich, F. Y. Gardes, and D. J. Thomson, "Silicon optical modulators," Nat. Photonics **4**(8), 518–526 (2010).
2. D. A. B. Miller, "Rationale and Challenges for Optical Interconnects to Electronic Chips," Proc. IEEE **88**(6), 728–749 (2000).
3. V. J. Sorger, R. F. Oulton, R.-M. Ma, and X. Zhang, "Toward integrated plasmonic circuits," MRS Bull. **37**(08), 728–738 (2012).
4. V. E. Babicheva, A. Boltasseva, and A. V. Lavrinenko, "Transparent conducting oxides for electro-optical plasmonic modulators," Nanophotonics **4**(1), 165–185 (2015).
5. D. K. Gramotnev and S. I. Bozhevolnyi, "Plasmonics beyond the diffraction limit," Nat. Photonics **4**(2), 83–91 (2010).
6. Z. Liu, H. Lee, Y. Xiong, C. Sun, and X. Zhang, "Far-field optical hyperlens magnifying sub-diffraction-limited objects," Science **315**(5819), 1686 (2007).
7. S. V. Zhukovsky, O. Kidwai, and J. E. Sipe, "Physical nature of volume plasmon polaritons in hyperbolic metamaterials," Opt. Express **21**(12), 14982–14987 (2013).
8. Z. Jacob, L. V. Alekseyev, and E. Narimanov, "Optical Hyperlens: Far-field imaging beyond the diffraction limit," Opt. Express **14**(18), 8247–8256 (2006).
9. H. N. S. Krishnamoorthy, Z. Jacob, E. Narimanov, I. Kretzschmar, and V. M. Menon, "Topological transitions in metamaterials," Science **336**(6078), 205–209 (2012).
10. V. P. Drachev, V. A. Podolskiy, and A. V. Kildishev, "Hyperbolic metamaterials: new physics behind a classical problem," Opt. Express **21**(12), 15048–15064 (2013).
11. A. Poddubny, I. Iorsh, P. Belov, and Y. Kivshar, "Hyperbolic metamaterials," Nat. Photonics **7**(12), 948–957 (2013).
12. E. E. Narimanov and A. V. Kildishev, "Naturally hyperbolic," Nat. Photonics **9**(4), 214–216 (2015).
13. M. Y. Shalaginov, V. V. Vorobyov, J. Liu, M. Ferrera, A. V. Akimov, A. Lagutchev, A. N. Smolyaninov, V. V. Klimov, J. Irudayaraj, A. V. Kildishev, A. Boltasseva, and V. M. Shalaev, "Enhancement of single-photon emission from nitrogen-vacancy centers with TiN/(Al,Sc)N hyperbolic metamaterial," Laser Photonics Rev. **9**(1), 120–127 (2015).

14. C. L. Cortes, W. Newman, S. Molesky, and Z. Jacob, "Quantum nanophotonics using hyperbolic metamaterials," J. Opt. **14**(6), 063001 (2012).
15. I. Avrutsky, I. Salakhutdinov, J. Elser, and V. Podolskiy, "Highly confined optical modes in nanoscale metal-dielectric multilayers," Phys. Rev. B **75**(24), 241402 (2007).
16. M. Yan, L. Thylén, and M. Qiu, "Layered metal-dielectric waveguide: subwavelength guidance, leveraged modulation sensitivity in mode index, and reversed mode ordering," Opt. Express **19**(4), 3818–3824 (2011).
17. Y. He, S. He, and X. Yang, "Optical field enhancement in nanoscale slot waveguides of hyperbolic metamaterials," Opt. Lett. **37**(14), 2907–2909 (2012).
18. V. E. Babicheva, M. Y. Shalaginov, S. Ishii, A. Boltasseva, and A. V. Kildishev, "Finite-width plasmonic waveguides with hyperbolic multilayer cladding," Opt. Express **23**(8), 9681–9689 (2015).
19. S. Ishii, M. Y. Shalaginov, V. E. Babicheva, A. Boltasseva, and A. V. Kildishev, "Plasmonic waveguides cladded by hyperbolic metamaterials," Opt. Lett. **39**(16), 4663–4666 (2014).
20. E. I. Lyashko and A. I. Maimistov, "Linear guided waves in hyperbolic slab waveguide. Dispersion relations," arXiv preprint arXiv:1507.07253 (2015).
21. P. Berini, "Long-range surface plasmon polaritons," Adv. Opt. Photonics **1**, 484–588 (2009).
22. J. Valentine, S. Zhang, T. Zentgraf, E. Ulin-Avila, D. A. Genov, G. Bartal, and X. Zhang, "Three-dimensional optical metamaterial with a negative refractive index," Nature **455**(7211), 376–379 (2008).
23. D. Chanda, K. Shigeta, S. Gupta, T. Cain, A. Carlson, A. Mihi, A. J. Baca, G. R. Bogart, P. Braun, and J. A. Rogers, "Large-area flexible 3D optical negative index metamaterial formed by nanotransfer printing," Nat. Nanotechnol. **6**(7), 402–407 (2011).
24. X. Ni, Z. Liu, and A. V. Kildishev, nanoHUB: Photonics DB (Optical Constants, 2010).
25. M. J. Dodge, "Refractive properties of magnesium fluoride," Appl. Opt. **23**(12), 1980–1985 (1984).
26. P. G. Snyder, Y.-M. Xiong, J. A. Woollam, G. A. Al-Jumaily, and F. J. Gagliardi, "Graded refractive index silicon oxynitride thin film characterized by spectroscopic ellipsometry," J. Vac. Sci. Technol. A **10**(4), 1462 (1992).
27. V. E. Babicheva, R. Malureanu, and A. V. Lavrinenko, "Plasmonic finite-thickness metal-semiconductor-metal waveguide as ultra-compact modulator," Photon. Nanostructures **11**(4), 323–334 (2013).
28. J. Chen, G. A. Smolyakov, S. R. Brueck, and K. J. Malloy, "Surface plasmon modes of finite, planar, metal-insulator-metal plasmonic waveguides," Opt. Express **16**(19), 14902–14909 (2008).

1. Introduction

Photonic integrated circuits can provide higher bandwidth and smaller power consumption in comparison to their electronic counterparts [1]. Conventional dielectric waveguides have been developed for many years and were shown to be favorable for passive guiding of light [2]. As a next step, efficient active devices, such as nanolasers, modulators, and photodetectors are to be designed [3,4]. The addition of metallic components into active devices can bring additional benefits such as providing electrodes for applying bias, injecting carriers, or transferring heat. Furthermore, the metal structures can support surface plasmon polaritons (SPPs), hence, providing high confinement of electromagnetic field along metal-dielectric interface. The highly confined fields can enhance the interaction between an active medium and propagating light [5]. Multilayer metal-dielectric structures are of particular interest, because they support plasmon-polariton waves with extremely small effective wavelength [6,7].

Multilayer metal-dielectric structures with hyperbolic dispersion, so called hyperbolic metamaterials (HMMs), have received significant interest of late [8–14]. Various plasmonic waveguides comprised of a multilayer core and a dielectric cladding or a multilayer cladding and a dielectric core, including multilayers with hyperbolic dispersion, have been analyzed [15–20]. It was shown that even a non-optimized design of a dielectric core and HMM claddings with a small metal filling ratio [HIH waveguide, Fig. 1(a)] was able to attain performance unachievable with the conventional plasmonic waveguides (metal-insulator-metal and insulator-metal-insulator) [19].

Here we theoretically demonstrate a special regime of SPP propagation, which can be achieved only in the waveguides with HMM layers (one or two HMM-dielectric interfaces) provided that the transverse component of the HMM effective permittivity ε_{yy} matches the permittivity of dielectric ε_c. This matching of permittivities (and consequently mode indices of each separated layer) enables resonant coupling of the modes at the HMM-dielectric interface and consequently long-range propagation of SPPs (LR-SPPs) in the waveguide.

Previously, long-range propagation was studied either for a thin metal film (*e.g* [21]. and references there) or a thin metal-dielectric stack [15]. In both cases, long-range modes arise from the coupling (often referred to as hybridization) of the SPP mode on each interface (metal-insulator or multilayer-insulator). If the thin metal film is surrounded by the same dielectric ε_d, SPPs on both metal-dielectric interfaces are resonantly coupled, and the LR-SPP propagates with the effective mode index $n_{eff} \approx \varepsilon_d^{1/2}$. It should be mentioned that there is no analogue of such long-range regime for the SPPs propagating along a conventional single metal-dielectric interface, as the indices of the materials could not be matched. In contrast, the HMM layer can be designed to possess the required permittivity components along the propagation and transverse directions. Thus, the transverse component of the effective permittivity tensor can be easily matched with the permittivity of the core, so that resonant coupling can be achieved. To the best of our knowledge, the regime of long-range propagation of SPP mode at HMM-dielectric interface was neither proposed nor studied.

In this paper, we analyze both HMM-dielectric single interface and HMM-insulator-HMM (HIH) plasmonic waveguides and propose an approach to significantly increase the propagation length, while keeping the mode size at a reasonable level. In particular, we study the HIH waveguide with silver-magnesium-fluoride (Ag/MgF$_2$) multilayer claddings [Fig. 1(b)] and show a propagation length of 0.8 mm at 1.55 μm can be achieved for the waveguide with a 300 nm and 1 μm thickness of its core and cladding, respectively.
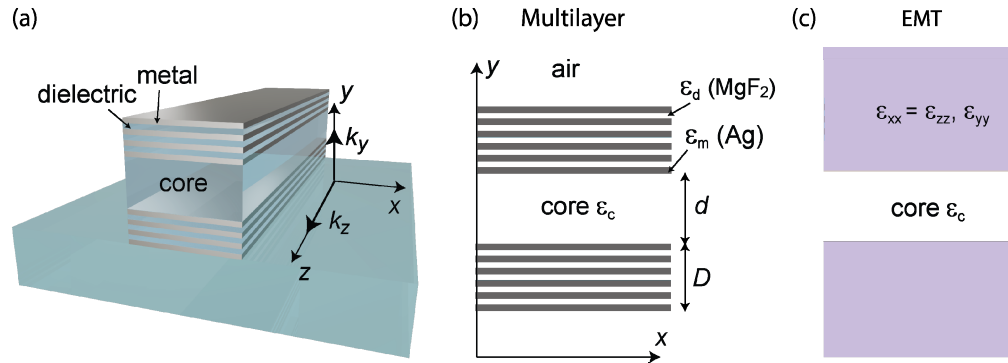

Fig. 1. (a) Schematic view of the HIH waveguide: the dielectric core is cladded by the metal-dielectric multilayer structure. (b) Structure under investigation (transverse cross-section): the multilayer structure consists of Ag and MgF$_2$ layers; core permittivity ε_c is varied. (c) Effective waveguide structure that corresponds to the HIH waveguide with the multilayer structure being replaced by an effective infinite medium with hyperbolic dispersion.

Following this analysis, Section 2 presents a study of the single HMM-dielectric interface built on the effective medium theory and the existence of long-range propagation of SPPs at the interface is demonstrated. Section 3 discusses the HIH plasmonic waveguide propagation length and mode confinement for the LR-SPP regime. We summarize the paper in Section 4. In the Appendix, we consider in more details the conditions for SPP mode localization and existence of long-range regime in the case of HMM-dielectric interface. In addition, we show analytical derivations for HIH structure.

2. Single HMM-dielectric interface

First, we study the long-range regime in the effective medium theory [EMT, Fig. 1(c)] approximation for the multilayer structure, which was shown to provide a reasonably good approximation [18,19]. In this approximation, the cladding can be modeled as a semi-infinite homogenous hyperbolic medium with effective-permittivity tensor components $\varepsilon_{xx} = \varepsilon_{zz} = r\varepsilon_m + (1-r)\varepsilon_d$ and $\varepsilon_{yy} = \left(r\varepsilon_m^{-1} + (1-r)\varepsilon_d^{-1} \right)^{-1}$, where ε_m and ε_d are metal and

dielectric permittivities, respectively, r is a metal filling ratio, $r = d_{\mathrm{m}}/(d_{\mathrm{m}} + d_{\mathrm{d}})$, d_{m} and d_{d} are the thicknesses of metal and dielectric layers, correspondingly [see Fig. 1(c)]. EMT calculations are performed in the same way as described in [19]. Wavelength λ_0 is chosen to be 1.55 μm (C-band telecom standard) and is fixed throughout the paper. We study a Ag/MgF$_2$ multilayer material with a filling ratio $r = 0.2$, as such combination was shown to be promising for plasmonic multilayer structures including negative index materials [22,23]. As metal and dielectric materials, we have chosen silver and MgF$_2$, the former because of its low loss, $\varepsilon_{\mathrm{m}} = \varepsilon_{\mathrm{Ag}} = -130.35 + 3.5i$ [24], and the latter has one of the lowest permittivities $\varepsilon_{\mathrm{d}} = \varepsilon_{\mathrm{MgF_2}} = 1.878$ [25]. Hence, according to EMT, the metamaterial permittivity tensor components are $\varepsilon_{xx} = \varepsilon_{zz} = -24.6 + 0.7i$ and $\varepsilon_{yy} = 2.35 + 0.0002i$. This metamaterial is often referred as type II or metallic type hyperbolic metamaterial [10,14]. The low permittivity of MgF$_2$ results in low ε_{yy}, which can be easily matched by conventional polymers and dielectrics, such as SiO$_2$ ($\varepsilon_{\mathrm{SiO_2}} = 2.25$) and silicon oxynitrides ($\varepsilon_{\mathrm{SiO_xN_y}} = 2.25\text{-}4$ [26]). Alternatively, the matching can be achieved by adjusting the metal filling ratio of the HMM, *i.e.*, tuning ε_{yy}. Here for simplicity we consider an infinitely wide (1D) waveguide. In a finite-width (2D) waveguide, we expect to observe additional transverse resonances, which were discussed in our previous work and should be avoided [18].

As a first step, we studied SPPs at a single HMM-dielectric interface, and in particular, we analyze dependences of propagation length and penetration depth on the dielectric permittivity ε_{c}. The SPP wave is set to propagate in z-direction. Inside HMM the wavevector $(0, k_{y,\mathrm{HMM}}, k_z)$ should satisfy the dispersion relation

$$\frac{k_z^2}{\varepsilon_{yy}} + \frac{k_{y,\mathrm{HMM}}^2}{\varepsilon_{zz}} = k_0^2, \tag{1}$$

where $k_0 = 2\pi / \lambda_0$ is a free-space propagation constant. The dispersion relation for SPP propagating inside the core is

$$k_z^2 + k_{y,\mathrm{diel}}^2 = \varepsilon_{\mathrm{c}} k_0^2, \tag{2}$$

where $k_{y,\mathrm{diel}}$ is a y-component of the wavevector in dielectric.

For a single interface of dielectric and HMM layer [Fig. 2(a)], the complex propagation constant is defined as

$$k_z = k_0 \left(\frac{\varepsilon_{\mathrm{c}}(\varepsilon_{zz} - \varepsilon_{\mathrm{c}})}{\varepsilon_{zz} - \varepsilon_{\mathrm{c}}^2 / \varepsilon_{yy}} \right)^{1/2}. \tag{3}$$

For the mode to be confined to the HMM-dielectric interface, the y-component of the propagation constant should satisfy the conditions:

$$k_{y,\mathrm{HMM}}^2 < 0 \text{ and } k_{y,\mathrm{diel}}^2 < 0. \tag{4}$$

Inequalities (4) are satisfied when $\varepsilon_{\mathrm{c}} < \mathrm{Re}[\varepsilon_{yy}]$ that follows from Eqs. (1) − (3) with $\mathrm{Re}[\varepsilon_{zz}] < 0$ (see more details in Appendix A1 and Fig. 6). The mode possesses a cut off, *i.e.* not bound to the interface if $\varepsilon_{\mathrm{c}} \geq \mathrm{Re}[\varepsilon_{yy}]$.

The propagation length of a given waveguide is defined through k_z of the waveguide mode as $L = \mathrm{Im}[2k_z]^{-1}$. We also define the penetration depth of the plasmonic mode into HMM and dielectric as $\delta_{\mathrm{HMM}} = \mathrm{Im}[2k_{y,\mathrm{HMM}}]^{-1}$ and $\delta_{\mathrm{diel}} = \mathrm{Im}[2k_{y,\mathrm{diel}}]^{-1}$, respectively, where $k_{y,\mathrm{HMM}}$ and

$k_{y,\text{diel}}$ are defined from Eqs. (1) and (2) through the propagation constant and permittivities. In Fig. 2(c), we have plotted the dependences of L and δ on core permittivity ε_c. L and δ drastically increase when $\varepsilon_c \rightarrow \text{Re}[\varepsilon_{yy}]$ (see more details in Appendix A2), this is where the long-range propagation regime is achieved. The propagation length in this regime can be on the order of hundreds of millimeters, which is two-three orders of magnitude larger than the propagation length of SPP at single metal-dielectric interface [Fig. 2(b), 2(c)].

As follows from Eq. (3), for $\varepsilon_c \rightarrow \text{Re}[\varepsilon_{yy}]$, SPP at the HMM-dielectric interface has a propagation constant $\text{Re}\,k_z \approx \varepsilon_{yy}^{1/2} k_0 \approx \varepsilon_c^{1/2} k_0$, which means $n_{\text{eff}} \approx \varepsilon_c^{1/2}$ and is similar to LR-SPPs existing in other geometries [15,21]. For $\text{Re}[k_z] \approx \varepsilon_{yy}^{1/2} k_0 \approx \varepsilon_c^{1/2} k_0$, both $k_{y,\text{HMM}}$ and $k_{y,\text{diel}} \rightarrow 0$, and SPP mode drastically extends [see Fig. 2(c)]. We note that for the multilayer structure, mode expansion means that resonant coupling between SPP of each layer inside HMM cladding is achieved (often referred to as bulk plasmon-polaritons), which causes long-range propagation of the HIH waveguide mode [see Fig. 2(d)].
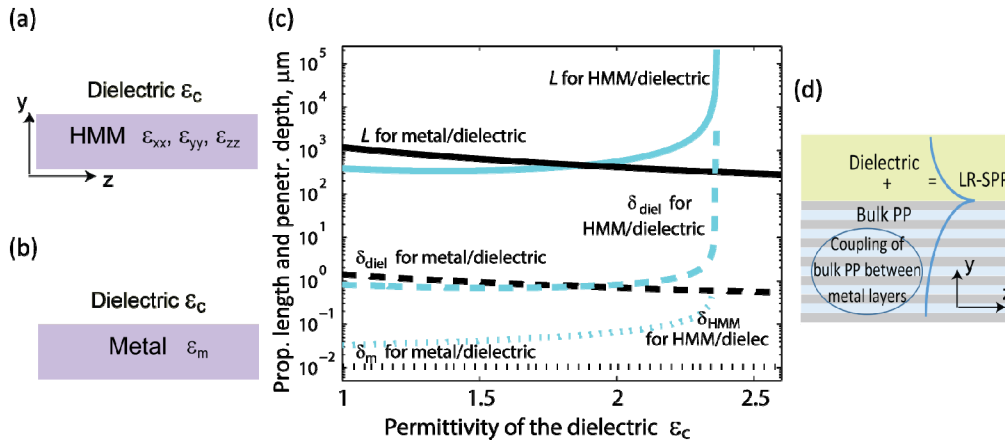

Fig. 2. Schematic view of (a) HMM-dielectric and (b) metal-dielectric single interfaces. (c) Propagation length L and penetration depth δ of SPPs for the HMM-dielectric and metal-dielectric single interfaces with varied dielectric permittivity. For the calculations of metal-dielectric case, the metal is the same as for the HMM (Ag). (d) Schematic view of the HMM-dielectric interface and resonant coupling of bulk plasmon-polaritons ("Bulk PP") inside HMM cladding to LR-SPP at the boundary.

3. HIH plasmonic waveguide

As a next step, we consider an HIH waveguide, which consists of a finite-size dielectric core cladded on both sides with HMMs. The conditions for long-range propagation are expected to be the same as for a single HMM-dielectric interface. However, the mode confinement of the HIH waveguide is anticipated to be increased. In this case, the expansion of the mode causes a strong coupling of the SPP on both HMM-dielectric interfaces, and for $\varepsilon_c \approx \text{Re}[\varepsilon_{yy}]$, an increase in propagation length, *i.e.* the long-range regime in HIH waveguides would be expected. To study LR-SPPs in the HIH waveguide, we calculated the dependence of propagation length L *vs.* core permittivity ε_c keeping the core thickness $d = 50$ nm. The calculation results shown in Fig. 3(a) confirm the presence of the long-range regime: for $\varepsilon_c \approx \text{Re}[\varepsilon_{yy}] \approx 2.35$, L possesses a strong increase up to 1.6 mm. Similar to the single interface, there are no confined modes at $\varepsilon_c > \text{Re}[\varepsilon_{yy}]$.

HIH waveguide mode under consideration is symmetric, which means that E_y and E_z are symmetric and antisymmetric in respect to waveguide center plane, correspondingly. In

general, multilayer metal-dielectric structure has been previously shown to support a variety of different plasmonic modes with rather complicated field profiles [15]. However, for the case $\varepsilon_c \approx \mathrm{Re}[\varepsilon_{yy}]$, our calculations show that the HIH waveguide does not support any other modes, and in particular no short-range antisymmetric SPP mode was found.

Further, we study the case of finitely-thick layers and finitely-thick cladding. The thicknesses of the metal and dielectric layers are chosen to be $d_m = 2$ nm and $d_d = 8$ nm, respectively, and the total thickness of the multilayer cladding from one side of the core is $D = 1$ μm. We perform our numerical simulations using a commercial finite element method (FEM) based eigenmode solver (CST Microwave Studio®) to calculate the complex propagation constant k_z of the waveguide mode. The blue curve in Fig. 3(a) shows tendency similar to the EMT calculations, *i.e.* there is an increase in L when ε_c approaches ε_{yy}. The maximum of L is shifted to lower permittivity values and is several times lower ($L_{max} = 0.6$ mm) in comparison to the case of semi-infinite EMT-approximated claddings. The reason for the maximum value existence is the following. When ε_c approaches ε_{yy}, the waveguide mode expands and finitely-thick cladding ($D = 1$ μm) starts to limit the mode. As a result, the solution is perturbed in comparison to the case of semi-infinite EMT-approximated cladding. It should be noted that in contrast to infinite cladding, in the case of finite thickness the solution does exist for $\varepsilon_c > \mathrm{Re}[\varepsilon_{yy}]$. In this region of ε_c values, the plasmon mode is confined by the boundaries of the multilayer cladding and does not experience a cut off.

In addition, we investigated the case of thicker cladding layers, in particular $d_m = 8$ nm and $d_d = 32$ nm. The results [purple curve in Fig. 3(a)] are similar to those in the previous case. The maximum of L for the "8/32 nm"-layer cladding is slightly lower and shifted more towards lower values of ε_c, in comparison to "2/8 nm"-layer cladding. The similarity between the results obtained for "8/32 nm" and "2/8 nm" claddings [purple and blue curves in Fig. 3(a)] suggests that layer thickness causes only slight modification.
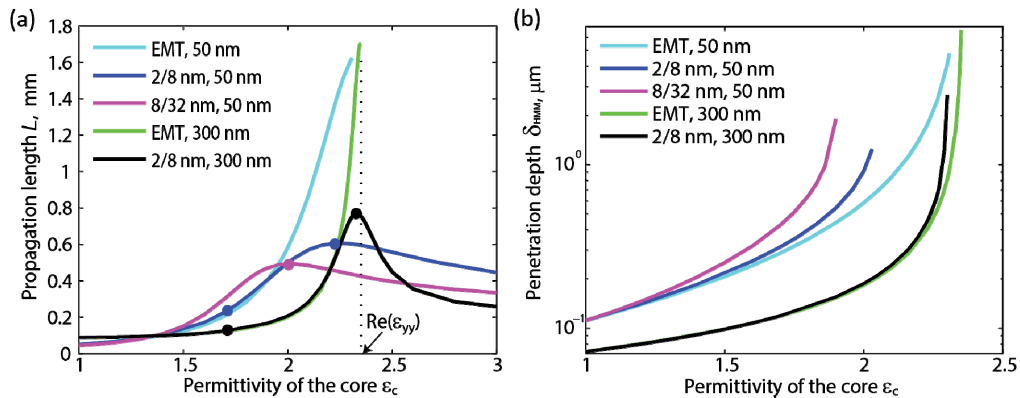

Fig. 3. (a) Propagation length L in the HIH waveguides in the case of semi-infinite EMT-approximated and 1-μm-thick multilayer cladding with different layer thicknesses. Core thickness d is 50 or 300 nm, and layer thicknesses $d_m = 2$ nm, $d_d = 8$ nm ("2/8 nm") or $d_m = 8$ nm, $d_d = 32$ nm ("8/32 nm"). Increase in propagation length L is observed for $\varepsilon_c \approx \mathrm{Re}[\varepsilon_{yy}]$. Circle marks on the curves designate core permittivity chosen for further analysis (see Fig. 5). (b) Penetration depth $\delta_{y,\mathrm{HMM}}$ of plasmonic mode into waveguide cladding *vs.* permittivity of the core ε_c. Waveguide parameters are the same as for (a).

To analyze the role of mode coupling between interfaces, we performed calculations for a thicker core $d = 300$ nm [green and black curves in Fig. 3(a)]. In this case, the multilayer claddings are placed further away, and the plasmon mode coupling inside the core is weaker than for the case of a thinner core with $d = 50$ nm. For $\varepsilon_c < 2.3$, mode is confined to core-

multilayer interface, and we observe the regime previously studied in [18,19]. For $1.4 < \varepsilon_c < 2.3$, the propagation length decreases as d increases (the blue curve is higher than the black one, IMI-like regime [19],), and for $\varepsilon_c < 1.4$, the propagation length increases as d increases (the blue curve is lower than the black one, MIM-like regime [19],). More detail analysis is shown in Appendix A3. When $\varepsilon_c \approx \text{Re}[\varepsilon_{yy}]$ long-range propagation regime takes place: modes on the both interfaces are highly hybridized, *i.e.* resonantly coupled, and the propagation length increases with an increase of d [maximum of the black curve is higher than the maximum of the blue curve in Fig. 3(a)]. Both EMT and finite-size cases [green and black curves in Fig. 3(a)] exhibit a similar behavior having a maximum for $\varepsilon_c \approx \text{Re}[\varepsilon_{yy}]$. An increase in propagation length is steeper for the thicker core, so for smaller ε_c, L is much smaller; but at the maximum, *i.e.* $\varepsilon_c \approx \text{Re}(\varepsilon_{yy})$, L_{max} is larger.

Further, we analyze the penetration depth $\delta_{y,\text{HMM}}$ of plasmon mode into the HMM cladding for different core permittivities ε_c [Fig. 3(b)]. We note that for rigorous numerical simulations of multilayer structure with FEM, $k_{y,\text{HMM}}$ are not defined, and we use Eqs. (1) for its calculation through k_z and effective material parameters. We plot $\delta_{y,\text{HMM}}$ only in the region where $\text{Re}(k_{y,\text{HMM}}^2) < 0$, which corresponds to the modes exponentially decaying inside the multilayer cladding in EMT approximation. For $\varepsilon_c > 1.8$, $\delta_{y,\text{HMM}}$ becomes relatively large in all cases. For the finite-size cladding, maximum of $\delta_{y,\text{HMM}}$ is limited by the cladding thickness and approximately equals to D (which is fixed to 1 μm). It explains the divergence of results for finite-thickness multilayers from EMT calculations [see Fig. 3(a)]. Steep increase in penetration depth agrees well with maximum of propagation length in Fig. 3(a). For $d = 300$ nm, the increase is much steeper and is observed for $\varepsilon_c \approx \text{Re}[\varepsilon_{yy}]$. Comparison of results in Fig. 2(c) and Fig. 3(b) shows that penetration depth in the case of HIH waveguide is at least one order of magnitude less than in the case of a single HMM–dielectric interface.

We calculate mode profiles to illustrate the long-range regime and the change of field distribution in the case of finite-thickness cladding (Fig. 4). E_y component of the mode field is symmetric in respect to the core center and has the same sign at the both sides of core-multilayer interface (symmetric-symmetric mode, Ss). Similar to E_y, E_z component of this mode does not change sign at the core-multilayer interface, but in contrast to E_y, E_z is antisymmetric in respect to the core center [Fig. 4(a)]. Thus, SPPs at both core-multilayer interfaces are coupled and enable long-range propagation. Detuning from the long-range regime [$\varepsilon_c = 1.7$, black curve in Fig. 4(a)] causes the mode to become more confined. If the waveguide cladding is thin, *e.g.* $D = 120$ nm [blue curve in Fig. 4(b)], the presence of the outer boundaries modifies the field significantly. Furthermore, similar to the case of metal-insulator-metal waveguide with thin layers [27], HIH waveguide with the thin cladding layers supports several modes of various symmetry. It essentially differs from the case of the infinitely thick cladding, where only symmetric-symmetric mode is supported. For example, in Fig. 4(c), we show the mode that is symmetric in respect to the core center, but changes sign at the core-multilayer interface (symmetric-antisymmetric mode, Sa). Although Sa mode has the highest confinement and provides the best conditions for field manipulation [27,28], the excitation of this mode in practical devices is problematic due to shorter propagation length and the antisymmetric mode profile.
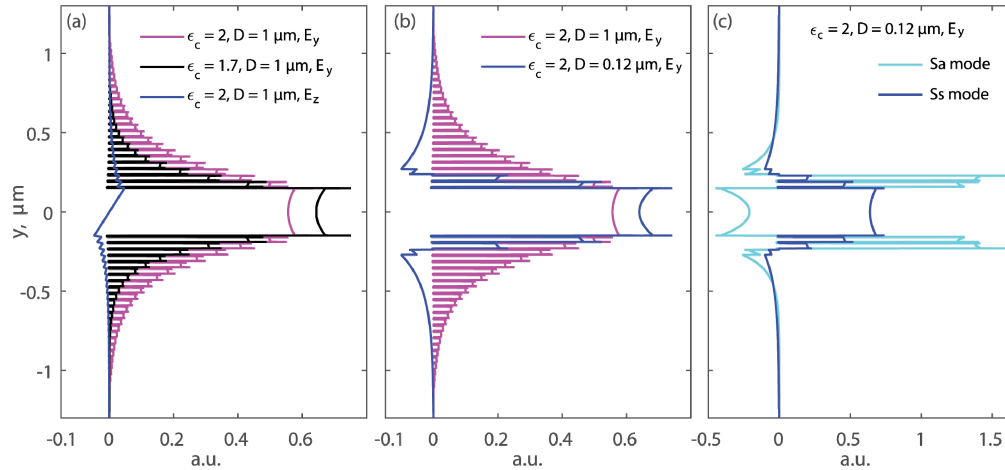
Fig. 4. Mode profiles for the core thickness $d = 300$ nm and layer thicknesses $d_m = 8$ nm and $d_d = 32$ nm. (a) The mode profiles (E_y field) at $\varepsilon_c = 2$ (purple curve) and $\varepsilon_c = 1.7$ (black curve) demonstrate the mode expansion when ε_c approaches $\mathrm{Re}[\varepsilon_{yy}] = 2.35$ (long-range regime). Antisymmetric mode profile of the E_z field is shown by the blue curve. (b) Change of the mode profile for the case of small D. (c) Symmetric-symmetric (Ss) and symmetric-antisymmetric (Sa) modes can exist in the HIH waveguide with the claddings of smaller thickness D.

Finally, we study the role of cladding thickness D for fixed values of ε_c [circle marks on the curves in Fig. 3(a)] by calculating L for different D up to 1 μm (Fig. 5). For $\varepsilon_c \approx \mathrm{Re}[\varepsilon_{yy}]$, *i.e.*, ε_c is equal to 2.3 for {2/8 nm, $d = 50$ nm}, 2 for {8/32 nm, $d = 50$ nm}, and 2.33 for {2/8 nm, $d = 300$ nm}, we observe monotonic increase in L, which means that the mode size is always limited by cladding thickness D. When ε_c is below the critical value $\mathrm{Re}[\varepsilon_{yy}]$, *i.e.*, $\varepsilon_c = 1.7$ for {2/8 nm, $d = 300$ nm} and {2/8 nm, $d = 50$ nm}, propagation length saturates at $D = 200$ nm and 1 μm, respectively. Hence, larger cladding thicknesses do not limit mode expansion. However, the maximum propagation length L_{max} is also lower (0.1 and 0.2 mm respectively).
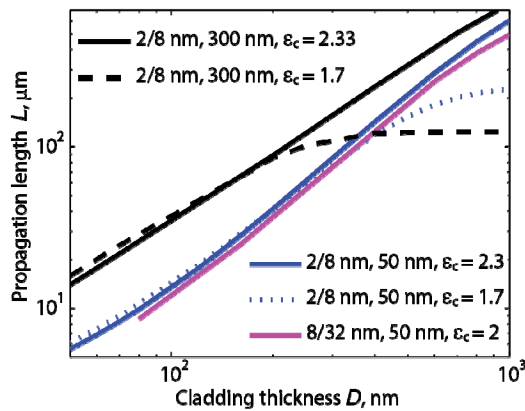

Fig. 5. The dependence of propagation length L on cladding thickness D for the HIH waveguide with parameters specified in the legend. For each line, the core permittivity ε_c is fixed and corresponds to circle marks shown in Fig. 3(a). Solid lines correspond to the maximums of the propagation length L_{max}.

4. Conclusion

To summarize, we studied the properties of plasmonic waveguides with a dielectric core and multilayer metal-dielectric claddings that possess hyperbolic dispersion. We analyzed the waveguide properties by varying the dielectric-core permittivity ε_c and calculating the propagation length for the multilayer structure with either 2/8-nm- or 8/32-nm-thick metal-dielectric layers and corresponding EMT approximations. Results showed that the propagation length is drastically increased when ε_c matches the ε_{yy}-component of the HMM cladding. Finite thickness of the cladding limits propagation length, which is also consistent with behavior of LR-SPPs. Our analysis with realistic materials shows that a propagation length of 0.5-0.8 mm can be achieved in the HIH waveguides.

Appendix

A1. Condition for SPP mode localization at the HMM-dielectric interface

For long-range propagation and significant mode expansion, complex k_y component may possess comparable real and imaginary parts. In this case, instead of inequalities (4), a more accurate condition for the SPP mode localization can be introduced:

$$\mathrm{Im}[k_y] \geq \mathrm{Re}[k_y]. \tag{5}$$

The condition is satisfied if $\varepsilon_c \leq \mathrm{Re}[\varepsilon_{yy}]$. The graphical representation of the inequality (5) is shown in Fig. 6.
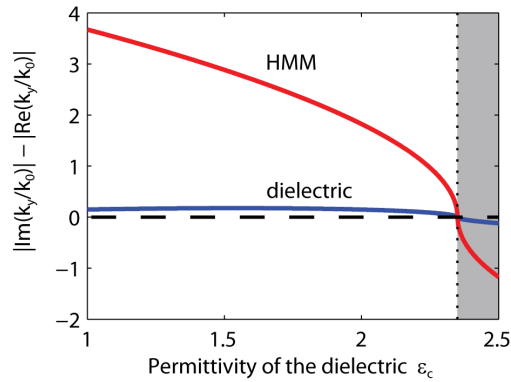

Fig. 6. Range of dielectric permittivities ε_c, where SPP mode propagating along HMM-dielectric interface can be considered as localized. Red and blue curves correspond to the HMM and dielectric semi-infinite media, respectively.

A2. Details of analytical study of the LR-SPP regime at the HMM-dielectric interface

A propagation length is defined as $L = \mathrm{Im}[2k_z]^{-1} \equiv \left(2k_z''\right)^{-1}$. The explicit expression of the real and imaginary parts of $k_z = k_z' + ik_z''$ given by Eq. (3) are the following:

$$k_z' = \left(\frac{1}{2}\left(\left[p^2 + q^2\right]^{1/2} + p\right)\right)^{1/2}, \tag{6}$$

$$k_z'' = \left(\frac{1}{2}\left(\left[p^2 + q^2\right]^{1/2} - p\right)\right)^{1/2}, \tag{7}$$

where

$$p = \varepsilon_c k_0^2 \frac{a(\varepsilon_{zz}' - \varepsilon_c) + \varepsilon_{zz}''}{a^2 + b^2},$$

$$q = \varepsilon_c k_0^2 \frac{a\varepsilon_{zz}'' - b(\varepsilon_{zz}' - \varepsilon_c)}{a^2 + b^2},$$

$$a = \varepsilon_{zz}' - \varepsilon_c^2 / \varepsilon_{yy}', b = \varepsilon_{zz}'' + \varepsilon_{yy}'' \varepsilon_c^2 / (\varepsilon_{yy}')^2.$$

From Eq. (7), the propagation length L approaches singularity when $q \to 0$. In the absence of transverse losses ($\varepsilon_{yy}'' = 0$), $q = k_0^2 \varepsilon_{zz}'' \varepsilon_c^2 \left(1 - \varepsilon_c / \varepsilon_{yy}'\right) / \left(a^2 + \varepsilon_{zz}''^2\right)$ turns to zero, when $\varepsilon_c = \varepsilon_{yy}'$ Taking into account transverse losses, a more accurate expression is $\varepsilon_c = \varepsilon_{yy}' \left(\frac{\varepsilon_{zz}'' \varepsilon_{yy}'}{\varepsilon_{zz}'' \varepsilon_{yy}' + \varepsilon_{zz}' \varepsilon_{yy}''} \right) = 2.357$. At this ε_c value, the plasmonic mode is quasi-localized and, in particular, $\Delta k_y = (\operatorname{Im} k_y - \operatorname{Re} k_y) / k_0$ is equal to −0.025 and −0.25 inside dielectric and HMM, respectively.

A3. Strong interaction of surface plasmon modes in HIH waveguide

The dispersion relations for 1D anisotropic waveguides and, in particular, HIH waveguide is given by (see Eq. (A9) in our previous work [19])

$$\tanh\left(\gamma_c \varepsilon_c \frac{d}{2} \right) = -\frac{\gamma_{\mathrm{HMM}}}{\gamma_c}, \tag{8}$$

where

$$\gamma_{\mathrm{HMM}} = \left(\varepsilon_{yy} \varepsilon_{zz}\right)^{-1/2} \left(k_z^2 - \varepsilon_{yy} k_0^2\right)^{1/2} \text{ and } \gamma_c = \varepsilon_c^{-1} \left(k_z^2 - \varepsilon_c k_0^2\right)^{1/2}.$$

For a small core thickness ($d \to 0$), $\tanh\left(\gamma_c \varepsilon_c d / 2\right)$ can be approximated as $\gamma_c \varepsilon_c d / 2$, and the solution of Eq. (8) can be expressed in the following way:

$$\frac{k_z}{k_0} = \left\{ \varepsilon_c + \frac{1}{2}\left[\frac{k_z^{(0)}}{k_0} \right]^2 + \left(\left[\frac{k_z^{(0)}}{k_0} \right]^2 \left(\varepsilon_c - \varepsilon_{yy} + \frac{1}{4}\left[\frac{k_z^{(0)}}{k_0} \right]^2 \right) \right)^{1/2} \right\}^{1/2}, \tag{9}$$

where

$$\frac{k_z^{(0)}}{k_0} = -\frac{2\varepsilon_c}{\left(\varepsilon_{zz}\varepsilon_{yy}\right)^{1/2}} \frac{1}{k_0 d}$$

is the propagation constant in the case of a very thin core. With the validity criterion $\gamma_c \varepsilon_c d \leq 1$, the approximation (9) is valid if $d < 700$ nm for the given HMM and dielectric core permittivities. Using analytically derived Eq. (9), we plotted a mode effective index $n_{eff} = \operatorname{Re}[k_z] / k_0$ and propagation length $L = \operatorname{Im}[2\mathrm{k}_z]^{-1}$ vs. dielectric core thickness d for various core permittivities ε_c (see Fig. 7). In the long-range regime ($\varepsilon_c = 2.35$), when the mode is highly extended into the claddings, the mode index and propagation length remain unchanged for d varied in the range of 10-500 nm. HIH waveguides possess a non-monotonous dependence of L on d: at smaller d values L becomes shorter as d increases (IMI-like behavior) and at larger d values the opposite way (MIM-like behavior).
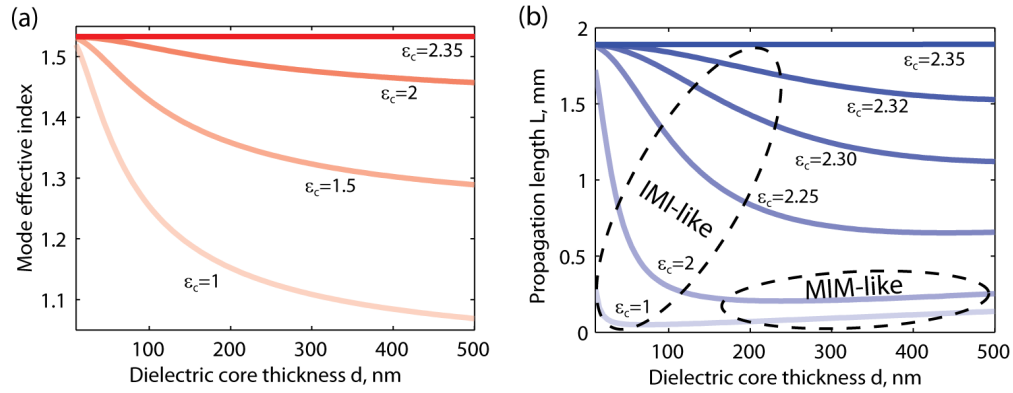
Fig. 7. (a) Mode effective index and (b) propagation length L *vs.* dielectric core thickness d for different values of core permittivity ε_c.

Acknowledgments